ISSN 1674-1056
http://cpb.iphy.ac.cn
http://iopscience.iop.org/cpb
中国物理 B
Chinese Physics
中国物理 Chinese Physics B

Growth and structural characteristics of metastable β-In_2Se_3 thin films on H-terminated Si(111) substrates by molecular beam epitaxy

Yi-Fan Shen(沈逸凡), Xi-Bo Yin(尹锡波), Chao-Fan Xu(徐超凡), Jing He(贺靖), Jun-Ye Li(李俊烨), Han-Dong Li(李含冬), Xiao-Hong Zhu(朱小红), Xiao-Bin Niu(牛晓滨)
Citation: Chin. Phys. B . 2020, 29(5): 056402 . **doi:** 10.1088/1674-1056/ab820f
Journal homepage: http://cpb.iphy.ac.cn; http://iopscience.iop.org/cpb

What follows is a list of articles you may be interested in

Structural transitions in $NaNH_2$ via recrystallization under high pressure

Yanping Huang(黄艳萍), Xiaoli Haung(黄晓丽), Xin Wang(王鑫), Wenting Zhang(张文亭), Di Zhou(周迪), Qiang Zhou(周强), Bingbing Liu(刘冰冰), Tian Cui(崔田)
Chin. Phys. B . 2019, 28(9): 096402 . **doi:** 10.1088/1674-1056/ab37f8

Pressure-induced isostructural phase transition in α-$Ni(OH)_2$ nanowires

Xin Ma(马鑫), Zhi-Hui Li(李志慧), Xiao-Ling Jing(荆晓玲), Hong-Kai Gu(顾宏凯), Hui Tian(田辉), Qing Dong(董青), Peng Wang(王鹏), Ran Liu(刘然), Bo Liu(刘波), Quan-Jun Li(李全军), Zhen Yao(姚震), Bing-Bing Liu(刘冰冰)
Chin. Phys. B . 2019, 28(6): 066402 . **doi:** 10.1088/1674-1056/28/6/066402

Calculation of the infrared frequency and the damping constant (full width at half maximum) for metal organic frameworks

M Kurt, H Yurtseven, A Kurt, S Aksoy
Chin. Phys. B . 2019, 28(6): 066401 . **doi:** 10.1088/1674-1056/28/6/066401

Study on the phase transition of the fractal scale-free networks

Qing-Kuan Meng(孟庆宽), Dong-Tai Feng(冯东太), Yu-Ping Sun(孙玉萍), Ai-Ping Zhou(周爱萍), Yan Sun(孙艳), Shu-Gang Tan(谭树刚), Xu-Tuan Gao(高绪团)
Chin. Phys. B . 2018, 27(10): 106402 . **doi:** 10.1088/1674-1056/27/10/106402

The effect of dislocations on the thermodynamic properties of Ta single crystal under high pressure by molecular dynamics simulation

Yalin Li(李亚林), Jun Cai(蔡军), Dan Mo(莫丹), Yandong Wang(王沿东)
Chin. Phys. B . 2018, 27(8): 086401 . **doi:** 10.1088/1674-1056/27/8/086401

Growth and structural characteristics of metastable β-In_2Se_3 thin films on H-terminated Si(111) substrates by molecular beam epitaxy*

Yi-Fan Shen(沈逸凡)[1], Xi-Bo Yin(尹锡波)[2], Chao-Fan Xu(徐超凡)[2], Jing He(贺靖)[2], Jun-Ye Li(李俊烨)[2], Han-Dong Li(李含冬)[2,†], Xiao-Hong Zhu(朱小红)[1,‡], and Xiao-Bin Niu(牛晓滨)[2]

[1] *College of Materials Science and Engineering, Sichuan University, Chengdu* 610064, *China*
[2] *School of Materials and Energy, University of Electronic Science and Technology of China, Chengdu* 610054, *China*

(Received 31 January 2020; revised manuscript received 14 March 2020; accepted manuscript online 23 March 2020)

Epitaxial growth and structural characteristics of metastable β-In_2Se_3 thin films on H-terminated Si(111) substrates are studied. The In_2Se_3 thin films grown below the β-to-α phase transition temperature (453 K) are characterized to be strained β-In_2Se_3 mixed with significant γ-In_2Se_3 phases. The pure-phased single-crystalline β-In_2Se_3 can be reproducibly achieved by *in situ* annealing the as-deposited poly-crystalline In_2Se_3 within the phase equilibrium temperature window of β-In_2Se_3. It is suggested that the observed γ-to-β phase transition triggered by quite a low annealing temperature should be a rather lowered phase transition barrier of the epitaxy-stabilized In_2Se_3 thin-film system at a state far from thermodynamic equilibrium.

Keywords: In_2Se_3, molecular beam epitaxy, single-crystalline, annealing and quench, phase transition

PACS: 64.60.My, 68.55.–a, 81.15.Hi, 68.35.Gy **DOI:** 10.1088/1674-1056/ab820f

1. Introduction

In_2Se_3 is an intriguing member of the group III_A–VI_A semiconductors with different phases and crystal structures, such as layered α-phase, layered β-phase, and defect wurtzite γ phase.[1] The most interesting and extensively studied phase of In_2Se_3 is layered α-phase, not only because of its superior optoelectric[2,3] and novel ferroelectric properties,[4–6] but also due a lot to its phase stability at normal pressure and temperature, thus it is widely fabricated by various thin film growth technologies.[7–10] In contrast to the α-In_2Se_3, the β- and γ-phases are metastable at normal pressure and temperature. The metastable In_2Se_3 phase shows more potential applications in serving as phase-change memorydevices,[11–15] though challenges remain in achieving these metastable phases (especially thin film structures for application purpose) with structural stability at normal pressure and temperature. Furthermore, the β-phase shows more excellent performance than the α-phase, especially in the optoelectric field. It has a larger photoresponse wavelength range and shorter photic response time to a ferroelectric polymer or $CuInSe_2$.[16,17] Meanwhile, the β-phase core field effect transistor also shows a higher field effect electron mobility, a higher carrier sheet density and a lower contact resistance than α-phase core field-effect transistor.[18]

Until now, there have been only a few references on the preparation of β- and γ-In_2Se_3 thin films. The γ-In_2Se_3 was grown by molecular beam epitaxy (MBE).[19,20] Compared with metastable γ-In_2Se_3, the β-In_2Se_3 exhibits a much lower phase equilibrium temperature; therefore, the phase-change memory devices at ambient temperatures are more appealing. It was reported that β-In_2Se_3 thin films could be synthesized from elemental In and Se sources by pulsed laser deposition (PLD) technique[21] or from γ-InSe compound sources by physical vapor transport (PVT) technique.[22] The β-In_2Se_3 could also be obtained through chemical routes such as chemical vapor deposition (CVD) technique.[23] Nevertheless, almost no research work has been reported on achieving controllable high-quality β-In_2Se_3 thin films.

In this work, we attempt to prepare metastable β-In_2Se_3 thin film by MBE. However, the direct MBE growth of In_2Se_3 within the phase equilibrium temperature window of β-In_2Se_3 (below 573 K) leads irreversible γ-phase In_2Se_3 to form. Hence, a growth strategy involving the low-temperature MBE deposition plus *in situ* post-deposition annealing is developed in order to suppress undesired γ-phase nucleation and then to achieve phase-pure β-In_2Se_3. It is demonstrated that the In_2Se_3 thin films grown from room temperature (RT) to 453 K are poly-crystalline, consisting of strained β-In_2Se_3 and a small quantity of γ-In_2Se_3 phases. It is very interesting to note that the post-annealing of the as-deposited poly-crystalline In_2Se_3 thin layer at a temperature ($\sim$ 573 K) much lower than

*Project supported by the National Key Research and Development Program of China (Grant Nos. 2018YFA0306102 and 2018YFA0306703), the National Natural Science Foundation of China (Grant Nos. 61474014 and U1601208), and the Sichuan Science and Technology Program, China (Grant Nos. 2019YJ0202 and 20GJHZ0229).

†Corresponding author. E-mail: hdli@uestc.edu.cn
‡Corresponding author. E-mail: xhzhu@scu.edu.cn

© 2020 Chinese Physical Society and IOP Publishing Ltd

the β-to-γ phase transition point (623 K) results in the formation of single-crystalline β-In_2Se_3 without any impure phases, suggesting full strain relaxation of the pristine β-In_2Se_3 phase and an uncommon phase transition path from γ to β phase in the In_2Se_3 film. The phase transition kinetics in the epitaxially quenched In_2Se_3 layer upon being annealed is discussed for depicting the observed uncommon phase transition phenomenon.

2. Experimental procedures

The growth of In_2Se_3 thin films was carried out in a customized MBE chamber with a base pressure of $\sim 3 \times 10^{-10}$ mbar (1 bar = 10^5 Pa). The Si(111) substrates were ultrasonically cleaned in acetone, alcohol, and deionized water in sequence for three rounds. Then they were deoiled in H_2SO_4 (98%) plus H_2O_2 (30%) solution. To remove the surface oxidized layer and obtain H-terminated surface, the cleaned Si substrates were etched in 40% HF solution for some minutes. Prior to growth, the H-terminated Si(111) substrates were degassed at a temperature below 453 K for 12 h. Ultrapure In ingot (99.9999+%) and Se pellets (99.999%) were evaporated from a standard Knudsen cell and a cracker cell, respectively. The beam equivalent pressure of In and Se were measured by a beam flux monitor. A large Se:In beam equivalent pressure ratio of $\sim 15:1$ was employed to ensure the Se-rich environment, which proved vital in our experiments for suppressing the formation of undesired InSe compound during growth. Since the epitaxial growth of layered selenides was fully cation dominated in any case,[24,25] the growth rate of In_2Se_3 thin films could be determined by the In flux. Accordingly, a growth rate of ~ 1 nm per min of In_2Se_3 film was achieved at an In beam equivalent pressure of 10×10^{-8} mbar, which was further confirmed by *ex situ* thickness measurements. The substrate temperature was measured by a thermocouple mounted near the substrate. The post-annealing procedure of as-deposited In_2Se_3 was held for 5 min then followed by a programmed quenching process. The surface structure evolution of In_2Se_3 during deposition was *in situ* monitored by reflection high energy electron diffraction (RHEED). The surface morphologies, crystallinities, and lattice vibration properties of obtained In_2Se_3 films were inspected by scanning tunnel microscopy (STM), high resolution x-ray diffraction (HRXRD), and Raman spectroscopy, respectively.

3. Results and discussion

Figure 1(a) shows a set of streaky 1×1 RHEED patterns from H–Si(111), indicating smooth morphology of H-passivated Si substrate after being etched in HF acid. Upon deposition, the In–Se film became amorphous, and then gradually crystallized as the growth procedure proceeded. Such an amorphous-to-crystalline transition at the initial stage of epitaxy was also observed during the growth of α-In_2Se_3 on H–Si(111).[10] The spotty RHEED patterns (Figs. 1(b) and 1(c)) suggest a typical island growth mode of the In–Se compound. Interestingly, the transmitted RHEED patterns manifest a zincblende structure of the islanded surface layer of In–Se. Such an islanded In–Se surface layer was observed to decorate on the growth front in the whole growth process. As is well known, the covalent selenides such as ZnSe usually crystallized into the wurzite or zincblende structure.[26] However, wurzite or zincblende In–Se did not exist in the In–Se phase diagram. Consequently, the epitaxial zincblende In–Se surface layer was inferred to be in a state that is far from thermodynamic equilibrium. The zincblende-type In–Se layer persisted on the surface of the In_2Se_3 film until the growth temperature was raised to higher than 453 K. Figure 1(d) shows a streaky 1×1 pattern of In_2Se_3 with the growth temperature raised to ~ 460 K. By carefully comparing the difference in streak spacing between substrate and epifilm, an in-plane lattice constant of ~ 4 Å was determined, which is nearly equal to the *a*-axis lattice constant of β-In_2Se_3. When the growth temperature was further increased to ~ 523 K, a set of $\sqrt{3} \times \sqrt{3}$ surface patterns gradually appeared with the in-plane lattice constant slightly increasing up to 4.1 Å, as depicted in Figs. 1(e) and 1(f), revealing the nucleation of γ-In_2Se_3 on the growth front. Although the surface morphology evolution was precisely monitored by RHEED, the structural characteristics of the epilayer beneath the growth front are still lacking. Hence, the HRXRD measurements were carried out in order to inspect thoroughly the structure of the as-deposited film. Figure 1(g) shows two typical XRD θ–2θ spectra for In_2Se_3 samples grown at relatively low temperatures (RT to 453 K) and high temperatures (453 K–573 K). Only (006) and (0012) diffraction peaks of γ-In_2Se_3 could be observed in the high temperature grown In_2Se_3 sample (red curve). While for the low temperature grown one, a series of XRD peaks from other phases were observed to coexist with those of the γ-In_2Se_3 phase (black curve). The positions of these XRD peaks, shifting to high angles as compared with the positions of the (00*n*) diffraction peaks of either α-In_2Se_3 or β-In_2Se_3, are closer to those of (00*n*) diffraction peaks of β-In_2Se_3. We thus speculate that the *c*-axis compressed β phase and γ phase coexisted in the low temperature grown sample. To support this hypothesis, Raman spectroscopy was used to further examine the lattice bonding nature and strain state of the epi-film. As shown in Fig. 1(h), there are no other peaks except the 150 cm^{-1} one that was observed in the high temperature grown sample (red curve) and belongs to the zone center mode of unstrained γ phase.[27] While in the low temperature grown sample, Raman peaks from both β- and γ-In_2Se_3 were observed (black

curve). The 148-cm^{-1} Raman peak of γ-In_2Se_3 was slightly blue-shifted, suggesting a strained state of γ-In_2Se_3 phase. However, the peaks at 109 cm^{-1} and 205 cm^{-1} matched well to those of unstrained β-In_2Se_3,[17] suggesting that the *c*-axis compressive strain, as revealed by XRD measurements, might be effectively accommodated within the van der Waals gaps, thus leaving the strong chemical bonds in the covalent cell of layered β-In_2Se_3 intact.

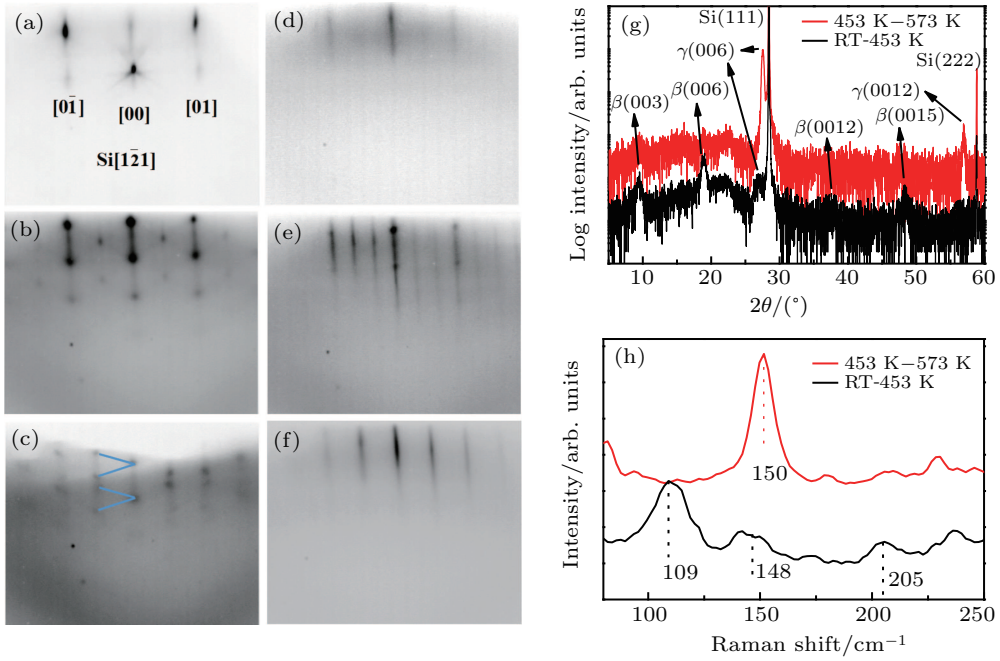


Fig. 1. (a) RHEED pattern of H-terminated Si(111) surface, taken along Si[1$\bar{2}$1] azimuth; (b) RHEED pattern of ZB-structure after the film growth, taken along Si[1$\bar{2}$1] azimuth; (c) RHEED pattern of ZB-structure after the film growth, taken along 30° rotating from Si[1$\bar{2}$1] azimuth, represented by blue lines; (d) RHEED pattern of growth beginning; (e) RHEED pattern after the film growth; (f) RHEED pattern after film growth taken along 30° rotating from Si[1$\bar{2}$1] azimuth; (g) XRD; (d) Raman spectra of In_2Se_3 thin films.

The growth of In_2Se_3 thin films is very complex under the non-equilibrium of thermodynamics in an MBE system, which contains strained β phase and further unexpected γ phase. The unexpected γ phase is stable after growth, indicating that an effective approach to crossing its growth temperature range (453 K–573 K) is required for obtaining the β phase. Therefore, a post-annealing treatment (at a temperature slightly higher than 573 K) followed by a rapid quench is used to drive the change of thermodynamically non-equilibrium state to a thermodynamically equilibrium state. The rapid quench rate is higher than 60 K/s. Figures 2(a)–2(d) illustrate the RHEED patterns after growth and post-annealing. The zincblende-structured In–Se surface exists in the whole growth process, while changing to a new pattern after the post-annealing and rapid quench treatment as shown respectively in Figs. 2(a) and 2(b). In Fig. 2(b), there are several bright points in the three stripes, which are an indicator of layered structure. The similar RHEED patterns can be seen along the Si[$\bar{1}$2$\bar{1}$] azimuth and by rotating 30° from Si[$\bar{1}$2$\bar{1}$] azimuth after post-annealing as shown in Figs. 2(c) and 2(d). The transformation in RHEED patterns demonstrates that the In_2Se_3 thin film actually changes into a layered structure by the post-annealing and rapid quench treatment. Furthermore, it is revealed by XRD spectra in Fig. 2(e) that the In_2Se_3 thin film changes from poly-crystalline to single-crystalline by the post-annealing and rapid quench treatment with all the relevant peaks becoming narrower and showing higher intensity. Likewise, the peak related to γ (006) is not observable after the rapid quench. The lattice constant of rapidly quenched sample is calculated to be 3.99 Å by RHEED patterns, which is very close to that of standard β phase (4.00 Å). Hence, it is supposed that a strain relaxation of β phase occurs after the post-annealing and rapid quench treatment. In addition, the Raman spectra are tested with data shown in Fig. 2(f). The blue shifts of peaks at 109 cm^{-1} (shifted to 110 cm^{-1}) and 205 cm^{-1} (shifted to 207 cm^{-1}), both of which are related to the A_1(LO + TO) symmetry mode of β phase, demonstrate again the strain relaxation of β phase after the post-annealing and rapid quench process. Meanwhile, the peak at 148 cm^{-1}, which is related to the zone center mode of γ phase, disappears after the heat treatment. As a consequence, both the XRD and Raman spectra evidence the phase transition from a mixture of strained β phase and γ phase to a pure β phase, driven by the "post-annealing and rapid quench"-induced strain relaxation.

To better understand the influence of quench rate, a further experiment is performed and then a representative sample is obtained. This sample experiences a slow quench (The quench rate is lower than 10 K/s) by keeping the other conditions the same as those for the rapidly quenched sample. It is witnessed that similar RHEED patterns are achieved after

the post-annealing and quench. But some differences cannot be neglected in the subsequent XRD and Raman characterizations. Figure 2(g) shows the XRD θ–2θ scan patterns of rapidly and slowly quenched In_2Se_3 samples. The diffraction peaks of slowly quenched sample lie between standard α-In_2Se_3 (JCPDS 34-0455) and β-In_2Se_3. All the high index peaks, such as (0015), exhibit obviously a left shift (red line), compared with those correponding peaks of the rapidly quenched sample, which indicates that this sample contains the α-In_2Se_3. Moreover, all the peaks are broadened and none of the peaks are split in the XRD spectrum, which further indicates that this sample is a mixture of α-In_2Se_3 and β-In_2Se_3. The peak broadening of (006) is also observed in a precise scan of omega-2 theta mode as shown in Fig. 2(h). The full width at half maximum (FWHM) of XRD profile for slowly quenched sample is much larger than that of rapidly quenched counterpart and these two peaks are both well distributed. The Raman spectra of the rapidly and slowly quenched samples demonstrate the same trend as shown in Fig. 2(i). A peak broadening at 108 cm^{-1} is noticed for the slowly quenched sample, which is related to the combination of peaks from α-In_2Se_3 (104 cm^{-1}) and β-In_2Se_3 (110 cm^{-1}). Likewise, the peak at 203 cm^{-1} is indexed to the combination of A_1(LO+TO) symmetry mode from α-In_2Se_3 and β-In_2Se_3.[18] This result is in good agreement with the XRD spectrum.

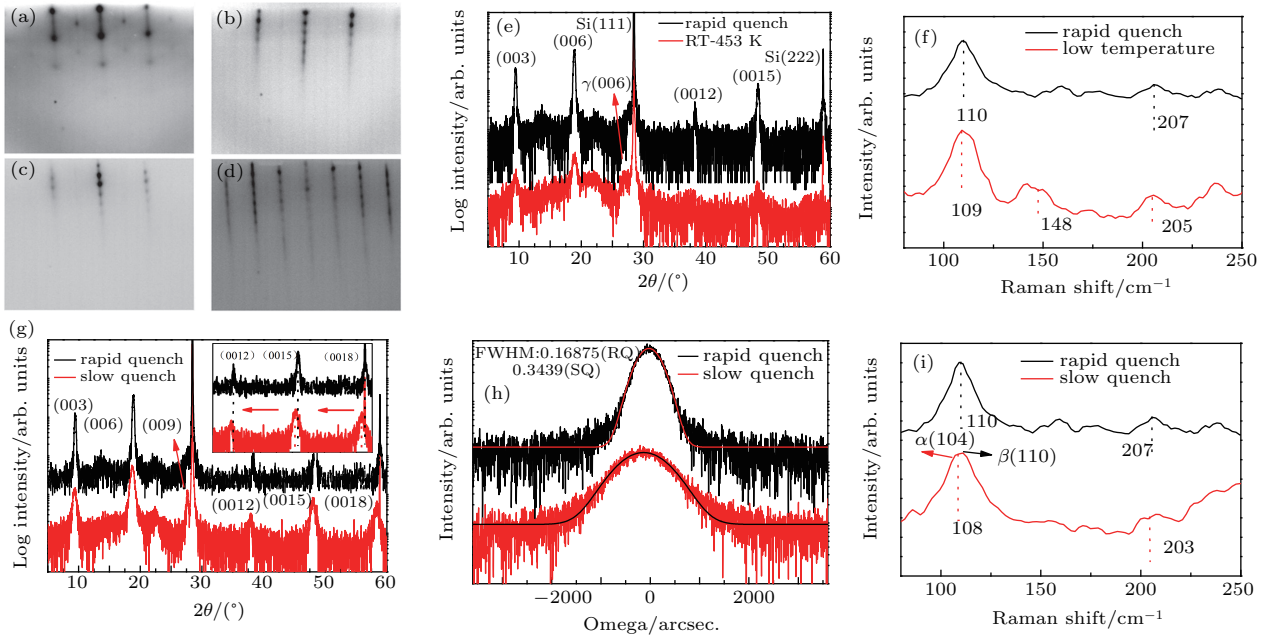


Fig. 2. (a) RHEED pattern of ZB-structure; RHEED patterns after the post-annealing, taken along (b) Si[$1\bar{2}$ 1] azimuth, (c) Si[$\bar{1}2\bar{1}$] azimuth, and (d) rotating 30° from Si[$\bar{1}2\bar{1}$] azimuth; (e) XRD spectra of low temperature grown sample and rapidly quenched sample; (f) Raman spectra of low temperature grown sample and rapidly quenched sample; (g) XRD spectra of slowly and rapidly quenched samples; (h) precise XRD spectra of β (006) diffraction peak for slowly and rapidly quenched samples; (i) Raman spectra of slowly and rapidly quenched samples.

After the post-annealing and rapid quench, the sample is further tested with STM. Typical morphology images of rapidly quenched In_2Se_3 sample are obtained as shown in Figs. 3(a) and 3(b). In the image on a large scale (see Fig. 3(a)), a featured morphology with crystalline grains arranged by steps is clearly seen. The orientation of thin film is consistent in the plane, which is represented by green triangles in Fig. 3(a). There is a flat area in the top part as shown in Fig. 3(b). Accordingly, a distance measurement across the step is obtained on a small scale with data shown in Figs. 3(c) and 3(d). In these images, the step height is measured to be 0.958 nm, which is very close to the thickness of a quintuple layer (1 QL = 0.95 nm–0.97 nm[28]) in the β-In_2Se_3. Thus, it is demonstrated that the sample after rapid post-annealing process is still composed of layered β-In_2Se_3 although the overall morphology is rough.

The coexistence of strained β phase and γ phase in the low temperature grown sample is believed to stem from the multiple random nucleations on the initial amorphous growth and in the subsequent nucleus growth process. The strain of β phase in that sample might originate from the H-terminated Si(111) substrate. There is a large lattice mismatch of 4.2% between β-In_2Se_3 and Si(111) in a axis (β-In_2Se_3: 4.00 Å, Si(111): 3.84 Å). Under such a circumstance, the lattice constant along the a axis is supposed to be smaller than 4.00 Å for the strained β phase, whereas the lattice constant along the c axis is also smaller as revealed already by the right shift in the XRD spectrum of low temperature grown sample. As a result, the unit-cell volume of strained β phase is compressed by $\sim$ 3.8% compared with that of the standard β phase. A similar volume decrease can be found in a previous research report,[29] in which it is reported that α

phase has an interlayer-glide-driven isosymmetric phase transition to β phase with a volume decrease of $\sim 7\%$ in the high pressure environment (0.8 GPa). Therefore, the strained β phase might be a kind of metastable phase arising from the thermodynamically non-equilibrium growth, and the thin epi-film is fully relaxed to single-crystalline β-In_2Se_3, which is driven by the strain relaxation after post-annealing. Furthermore, it can be observed in the Raman spectra that the peaks present blue shift, implying a collapse of epitaxial equilibrium and an expansion of volume after post-annealing. Meanwhile, the γ phase also transforms into β-In_2Se_3 phase after post-annealing, no matter the quench is rapid or slow. It is verified in the Raman spectra, as shown in Fig. 2(h), that the peak at 148 cm^{-1}, which belongs to the γ phase, cannot be observed for the post-annealed sample. Thus, an uncommon γ-to-β phase transition occurs in our In_2Se_3 thin film. The phase transitions in In_2Se_3 generally stem from some high temperature or pressure effects. A previous article[12] indicated that the α-In_2Se_3 phase changes into β-In_2Se_3 after post-annealing at 573 K and the β-In_2Se_3 phase is stable. A similar experiment was also conducted by another research group,[18] while the temperature used (623 K) was higher. These two articles demonstrate that the β-In_2Se_3 is stable when it came from a high temperature environment or a post-annealing process. An uncommon γ-to-β phase transition was similarly observed in the high pressure environment (3.2 GPa to 3.7 GPa), as reported previously,[30] which demonstrated that the β phase was more stable than the γ phase in the high pressure environment and such a phase transition was not reversible. The similar phase transition was also observed with other material systems in the high pressure environment.[31] The uncommon phase transition observed in this work might originate from more complicated reasons, which will be studied systematically in our future work.

The high rate of quench proves to be important to retain the single crystal quality of β-In_2Se_3 thin films. It is verified that a non-strained-β-to-α-phase transition happens in the slow quench process, which is observed in the precise omega-2 theta scan as already shown in Fig. 2(h). The obvious broadening at (006) peak of the slowly quenched sample indicates that the In_2Se_3 phase of this sample is an intermediate state during phase transition, coming probably from the short-range diffusion, which is however not a nucleation. This phase transition, which is ascribed to the slow quench with temperature gradually decreasing down to room temperature (passing through the β-to-α phase transition point), can be regarded as a spinodal-type process.[32] The rapid quench ends in less than 5 s, thereby suppressing kinetically the transition from non-strained β to α phase, while the slow quench promotes the short-range diffusion. Therefore, if single-crystalline β-In_2Se_3 thin films are desired, the rate of quench should be as high as possible to avoid the existence of α phase, thereby demonstrating that the non-strained β-In_2Se_3 after post-annealing is completely retained by the rapid quench, giving an important reference to obtaining single-crystalline β-In_2Se_3 thin films.

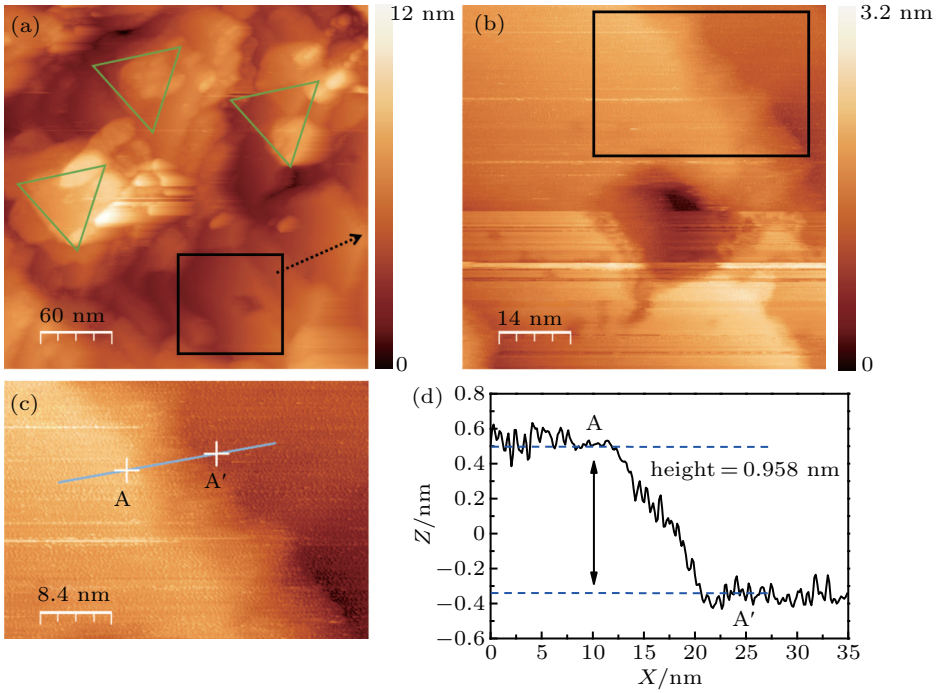


Fig. 3. STM images of 30-nm-thick In_2Se_3 thin film with post-annealing and rapid quench, showing (a) surface morphology in a large scale of 300 nm×300 nm; (b) surface morphology in a medium scale of 70 nm×70 nm, represented by black square in panel (a); (c) surface morphology with a step in small scaled area 42 nm×30 nm, represented by the black rectangle in panel (b); (d) step height is characterized to be 0.958 nm after correction.

4. Conclusions

In this work, single-crystalline β-In_2Se_3 thin films are obtained by a low temperature MBE growth (below 453 K) followed by post-annealing and rapid quench. When the growth temperature is below 453 K, the samples are In_2Se_3 thin films with strained β-In_2Se_3 and γ-In_2Se_3 co-existing. When the temperature is above 453 K but lower than 573 K, the samples are completely γ-In_2Se_3 thin films. Very importantly, beginning with a low temperature growth (below 453 K) and then post-annealing at a temperature slightly higher than 573 K together with rapid quench, a single-crystalline β-In_2Se_3 thin film sample can be obtained. It is speculated that the transition from a mixture of strained β and γ phases to a pure β phase is driven by the strain relaxation with post-annealing and rapid quench. Eventually, a high rate of quench is the key to avoiding the spinodal-type-β-to-α-phase transition.

References

[1] Han G, Chen Z G, Drennan J and Zou J 2014 *Small* **10** 2747
[2] Island J O, Blanter S I, Buscema M, Van der Zant H S J and Castellanos-Gomez A 2015 *Nano Lett.* **15** 7853
[3] Jacobs-Gedrim R B, Shanmugam M, Jain N, Durcan C A, Murphy M T, Murray T M, Matyi R J, Moore R L and Yu B 2014 *ACS Nano* **8** 514
[4] Ding W J, Zhu J B, Wang Z, Gao Y F, Xiao D, Gu Y, Zhang Z Y and Zhu W G 2017 *Nat. Commun.* **8** 14956
[5] Cui C J, Hu W J, Yan X X, Addiego C, Gao W P, Wang Y, Wang Z, Li L Z, Cheng Y C, Li P, Zhang X X, Alshareef H N, Wu T, Zhu W G, Pan X Q and Li L J 2018 *Nano Lett.* **18** 1253
[6] Poh S M, Tan S J R, Wang H, Song P, Abidi I H, Zhao X X, Dan J D, Chen J S, Luo Z T, Pennycook S J, Castro Neto A H and Loh K P 2018 *Nano Lett.* **18** 6340
[7] Zhai T Y, Fang X S, Liao M Y, Xu X J, Li L, Liu B D, Koide Y, Ma Y, Yao J N, Bando Y and Golberg D 2010 *ACS Nano* **4** 1596
[8] Ho C H, Lin C H, Wang Y P, Chen Y C, Chen S H and Huang Y S 2013 *ACS Appl. Mater. Interfaces* **5** 2269
[9] Li Q L, Liu C H, Nie Y T, Chen W H, Gao X, Sun X H and Wang S D 2014 *Nanoscale* **6** 14538
[10] Li H D, Ren W Y, Wang G Y, Gao L, Peng R M, Li H, Zhang P Y, Shafa M, Tong X, Luo S Y, Zhou Z H, Ji H N, Wu J, Niu X B and Wang Z M 2016 *J. Phys. D: Appl. Phys.* **49** 145108
[11] Chen J, Du G and Liu X Y 2015 *Chin. Phys. B* **24** 057702
[12] Choi M S, Cheong B K, Ra C H, Lee S, Bae J H, Lee S, Lee G D, Yang C W, Hone J and Yoo W J 2017 *Adv. Mater.* **29** 1703568
[13] Pandiana M, Matheswarana P, Gokul B, Sathyamoorthy R and Asokan K 2018 *Appl. Surf. Sci.* **449** 55
[14] Lee H, Kang D H and Tran L 2005 *Mater. Sci. Eng. B* **119** 196
[15] Jin B, Kang D, Kim J, Meyyappan M and Lee J S 2013 *J. Appl. Phys.* **113** 164303
[16] Wu G J, Wang X D, Wang P, Huang H, Chen Y, Sun S, Shen H, Lin T, Wang J L, Zhang S T, Bian L F, Sun J L, Meng X J and Chu J H 2016 *Nanotechnology* **27** 364002
[17] Zheng Z Q, Yao J D and Yang G W 2017 *ACS Appl. Mater. Interfaces* **9** 7288
[18] Feng W, Gao F, Hu Y X, Dai M J, Liu H, Wang L F and Hu P A 2018 *ACS Appl. Mater. Interfaces* **10** 27584
[19] Chaiken A, Nauka K, Gibson G A, Lee H, Yang C C, Wu J, Ager J W, Yu K M and Walukiewicz W 2003 *J. Appl. Phys.* **94** 2390
[20] Okamoto T, Yamada A and Konagai M 1997 *J. Cryst. Growth* **175–176** 1045
[21] Zheng Z Q, Yao J D, Xiao J and Yang G W 2016 *J. Mater. Chem. C* **4** 8094
[22] Balakrishnan N, Staddon C R, Smith E F, Stec J, Gay D, Mudd G W, Makarovsky O, Kudrynskyi Z R, Kovalyuk Z D, Eaves L, Patanè A and Beton P H 2016 *2D Mater.* **3** 025030
[23] Zhou S, Tao X and Gu Y 2016 *J. Phys. Chem. C* **120** 4753
[24] Ren W Y, Li H D, Gao L, Li Y, Zhang Z Y, Long C J, Ji H N, Niu X B, Lin Y and Wang Z W 2017 *Nano Res.* **10** 247
[25] Li H D, Yu S P, Li Y, Channa A I, Ji H N, Wu J, Niu X B and Wang Z M 2019 *Appl. Phys. Lett.* **115** 041602
[26] Li H D, Wang Z Y, Guo X, Wong T L, Wang N and Xie M H 2011 *Appl. Phys. Lett.* **98** 043104
[27] Yuan Y F, Cao X R, Sun Y, Su J, Liu C M, Cheng L, Yuan L H, Zhang H and Li J 2017 *RSC Adv.* **7** 46431
[28] Zhang F, Wang Z, Dong J Y, Nie A M, Xiang J Y, Zhu W G, Liu Z Y and Tao C G 2019 *ACS Nano* **13** 8004
[29] Ke F, Liu C L, Gao Y, Zhang J K, Tan D Y, Han Y H, Ma Y Z, Shu J F, Yang W G, Chen B, Mao H K, Chen X J and Gao C X 2014 *Appl. Phys. Lett.* **104** 212102
[30] Rasmussen A M, Mafi E, Zhu W G, Gu Y and McCluskey M D 2016 *High Press. Res.* **36** 549
[31] Huang Y P, Huang X L, Wang X, Zhang W T, Zhou D, Zhou Q, Liu B B and Cui T 2019 *Chin. Phys. B* **28** 096402
[32] Li H D, Zhang X N, Zhang Z, Mei Z X, Du X L and Xue Q K 2007 *J. Appl. Phys.* **101** 106102